POSTER NR.: B712

Land subsidence, structures and processes at the Dead Sea shoreline

as revealed by a Near-field Photogrammetry survey at Ghor Haditha, Jordan

Djamil Al-Halbouni[1], Eoghan P. Holohan[1], Thomas Walter[1], Hussam Alrshdan[2], Leila Saberi[1], Ali Sawarieh[2], Torsten Dahm[1]

1. Helmholtz Centre - German Research Centre for Geosciences (GFZ), Potsdam, Germany (email: halbouni@gfz-potsdam.de) 2. Ministry of Energy and Natural Ressources, Jordan

1. Introduction

Rapid recession of the Dead Sea has led to dramatic sinkhole development around the lake shore (Yechieli et al., 2006). Such land subsidence phenomena pose a major hazard to local infrastructure, agriculture and industry.

Here, we focus on the Ghor Haditha sinkhole area in Jordan (**Fig. 1a**), which lies between two periodically active wadi systems, Ibn Hammad and Mutayl (**Fig. 1b**). Sinkholes have been reported as early as 1992 (Taqieddin et al., 2000). Sinkhole occurrence, morphology and temporal development in this area are nevertheless incompletely understood.

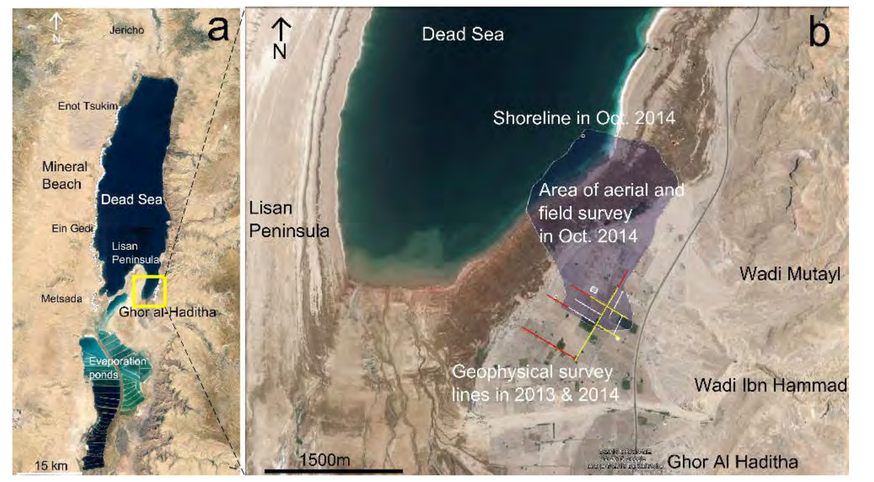

Figure 1: (**a**) Locations of Ghor Haditha and other areas of reported sinkhole occurrence at the Dead Sea, as indicated by white circles. (**b**) Setting of the sinkhole area of Ghor Haditha. Shaded area is that of the survey area. Note the shoreline recession of 200 m since 2011.

2. Methods: Fieldwork and Near-field Helikite Photogrammetry

To better understand sinkhole formation at Ghor Haditha, we conducted field investigations and a photogrammetric survey in October 2014.

Aerial images of the area were acquired by a 12 Megapixel camera mounted on a helium-filled balloon that flew at between 100 and 150 m altitude (**Fig. 2**). The photo footprint was about 100 x 120 m; ground resolution was around 3 cm/pixel. For geo-referencing, over 60 ground control points were measured by DGPS with up to 10 cm accuracy (**Fig. 3**).

The aerial images were aligned and 3D point clouds extracted by using the Structure-from-Motion photogrammetric method (Harwin and Lucieer (2012)), as implemented in the software AgisoftPro.

Figure 2: Reeling out the camera bearing Helikite balloon at the fractured edge of the alluvium sinkhole area.

Figure 3: Measuring the ground control points with a high accuracy DGPS (10 cm horizontal error).

3. Results I: Observations from Fieldwork and Aerial Photography

Geology

Figure 4: Alluvium fan deposits, comprising conglomerates, coarse to fine grained sand, with a clayey topsoil.

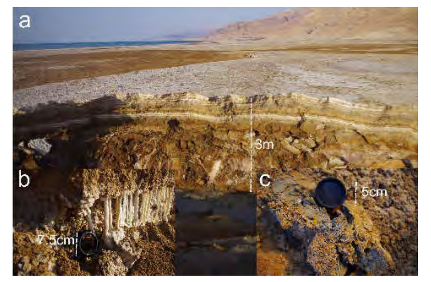

Figure 5: Mud-flat deposits, comprising (**a**) laminated silt and clay, locally interbedded with (**b**) evaporite layers up to 1.5 m thick. Ideomorphic halite crystals in clay (**c**).

Structures

Figure 6: Large normal fault scarps (ca. 1 m high) and cracks (ca. 4 m deep) in the rheologically strong alluvium.

Figure 7: Listric normal fault bounding back-rotated blocks of a landslide or slump in the rheologically weak mud-flat deposits.

Sinkholes

Figure 8: A typical 12 m deep and narrow sinkhole in the strong alluvium (**a**). Some even have overhanging sides (**b**).

Figure 9: Typical shallow (1.5 m) and wide sinkhole in the weak mud-flat deposits. Dashed line: alluvium/mud-flat contact.

Streams/subsurface flow

Figure 10: Stream channel in the mud-flat at the alluvium boundary (**a**). Evidence of channelized flow within the mud-flat sediments (**b**).

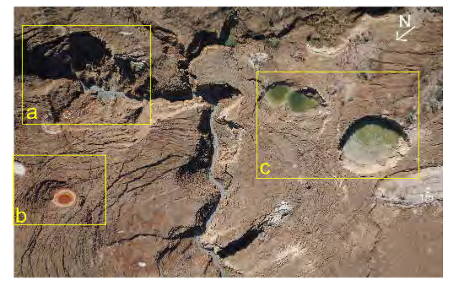

Figure 11: A sediment-laden stream emerges from within the mud-flat sediments (**a**). Sinkholes in the mud-flat filled by salt-water (**b**) or fresh/brackish water (**c**).

The area contains two main geological units: (**1**) **old, conglomeratic alluvial fan deposits (alluvium)** and (**2**) **interbedded lacustrine clay and evaporite deposits (mud-flat)**; the latter represents the former Dead Sea bed (**Figs. 4** and **5**). The alluvium is rheologically strong and supports brittle deformation (**Fig. 6**). The clay/evaporite sequence in contrast reveals a more brittle-ductile deformation (**Fig. 7**) and comprises soluble deposits of aragonite, gypsum and halite. Correspondingly, **sinkholes in the mud-flat and the alluvium appear morphologically different** (Figs. **8** and **9**).

Several stream channels dissect the mud-flat (**Fig. 10**). Most of these were dry at the time of our survey. However, an active stream that formed in early 2014 was also observed. This rises from within the mud-flat sediments at around 6 m below the surface (**Fig. 11a**). These springs appear at the major depression zone in the central part of the surveyed area. The water flows either in large canyons or as subterranean channels beneath the mud (**Fig. 10**).

The mud-flat also exhibits several slump-related seeps, at least one small cave stream (**Fig. 10b**) and several water-filled sinkholes (some vegetated) that partially exhibit salt rims (**Fig. 11b, c**).

4. Results II: Orthophoto and Digital Elevation Model

The preliminary orthophoto (**Fig. 12**) and digital elevation model (DEM) (**Fig. 13**) shown here for the surveyed area were constructed from ca. 20 % of a total of ca. 13000 images. The orthophoto resolution is 10 cm/pixel. The DEM resolution is up to 5 cm with an accuracy of around 25 cm.

Comparison of orthophoto and the DEM of the survey area reveals several important **morphological features**:

Firstly the stream channels cutting the mud-flat do not continue onto the alluvium. Rather, the **heads of these channels (several vegetated) occur at the mud-flat/alluvium boundary**. Together with the outcrop observations in section 3, there is therefore strong evidence for subsurface flow of relatively fresh groundwater both from within the alluvium onto the mud-flat and within the mud-flat sediments themselves.

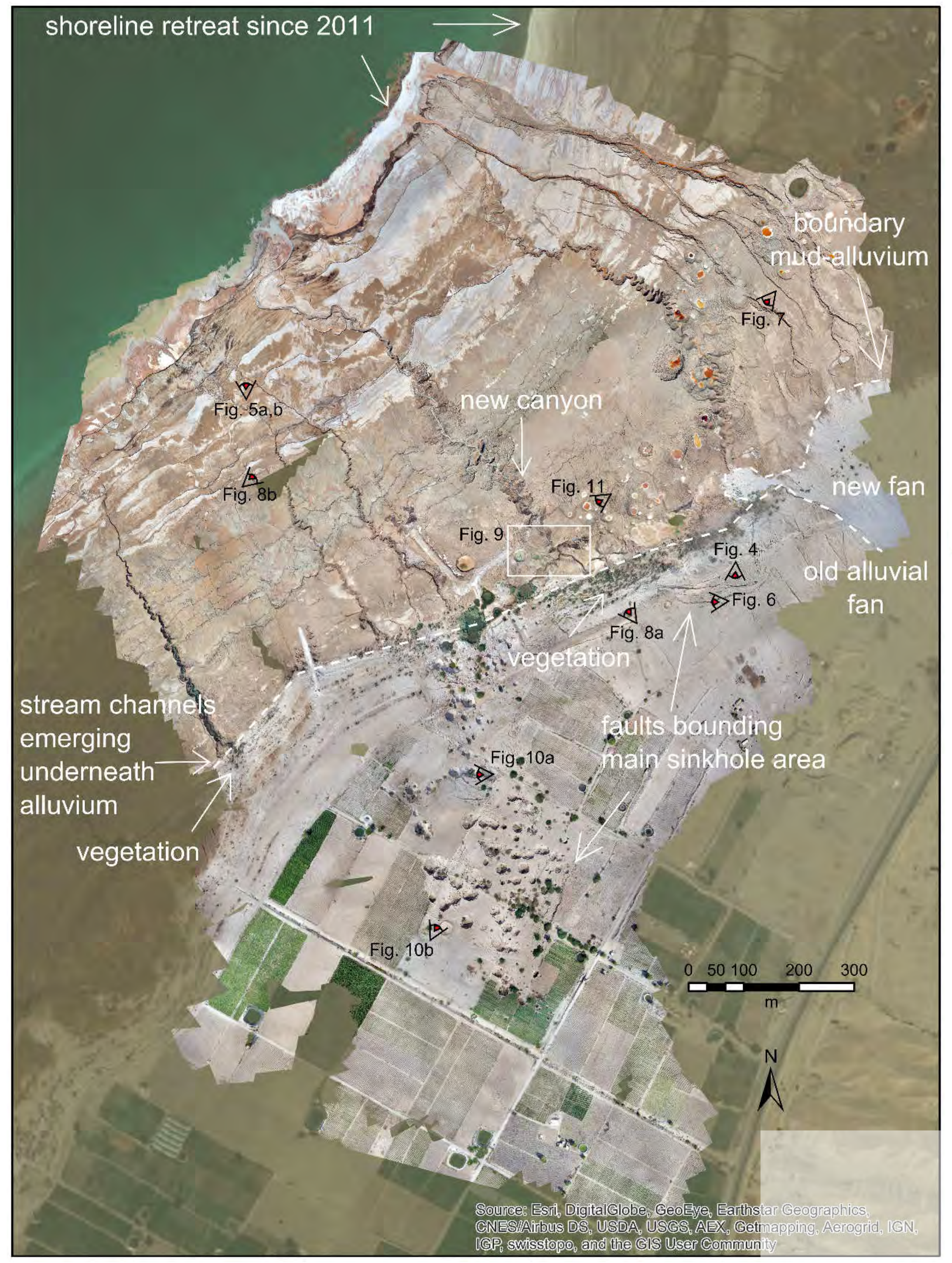

Figure 12: High resolution (10 cm/pixel) Orthophoto of Ghor Haditha sinkhole area with satellite image background. Indicated are the most important morphological features as well as the locations where field observation photos of section 3 were taken. This dynamically changing area comprises very recently formed channels and alluvial fans in the central and eastern part.

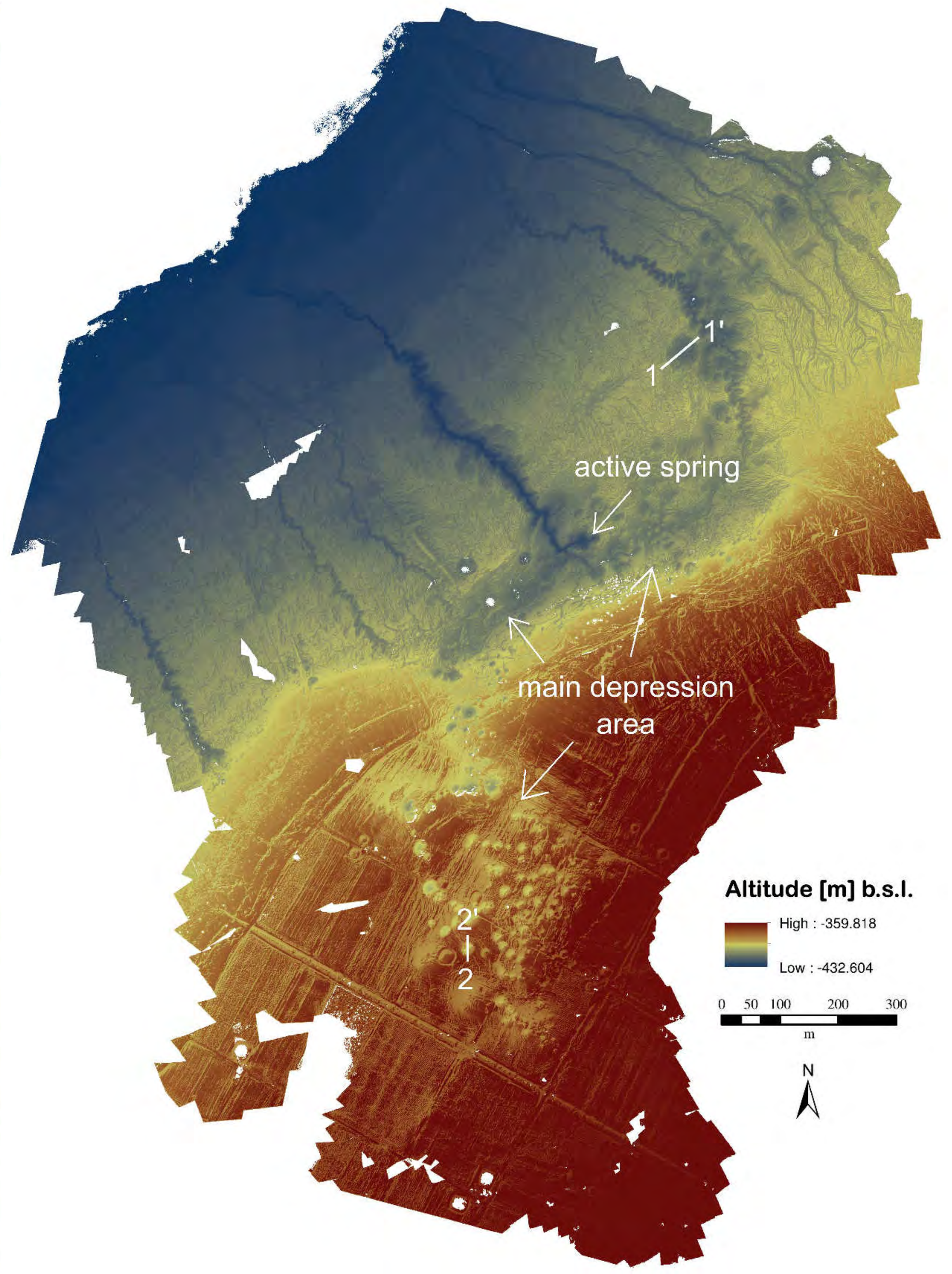

Figure 13: Shaded relief image with overlain topography at Ghor Haditha sinkhole area resulting from the digital elevation model. The main depression area, the active groundwater spring and the location of topographic profiles shown in section 5 are indicated. A further continuation of the major depression zone to the NE can be inferred from the DEM and satellite images.

Secondly, most of the sinkholes in the surveyed area are clustered into a roughly NNW-SSE orientated zone on the alluvium and in a ENE-WSW orientated zone straddling the alluvium/mud-flat boundary (**Fig. 12**). The DEM shows that these two zones form a **subtle, large-scale, sinuous depression** (**Fig. 13**). The faults and fractures observed in the alluvium are located at and follow the boundary of this depression.

Finally, the active stream in the area emerges from the center of the ENE-WSW elongated section of the main depression. This indicates that the occurrence of the main depression, and the sinkholes within it, are primarily controlled by **channelized subsurface ground water flow**.

5. Results III: Geomorphological analysis

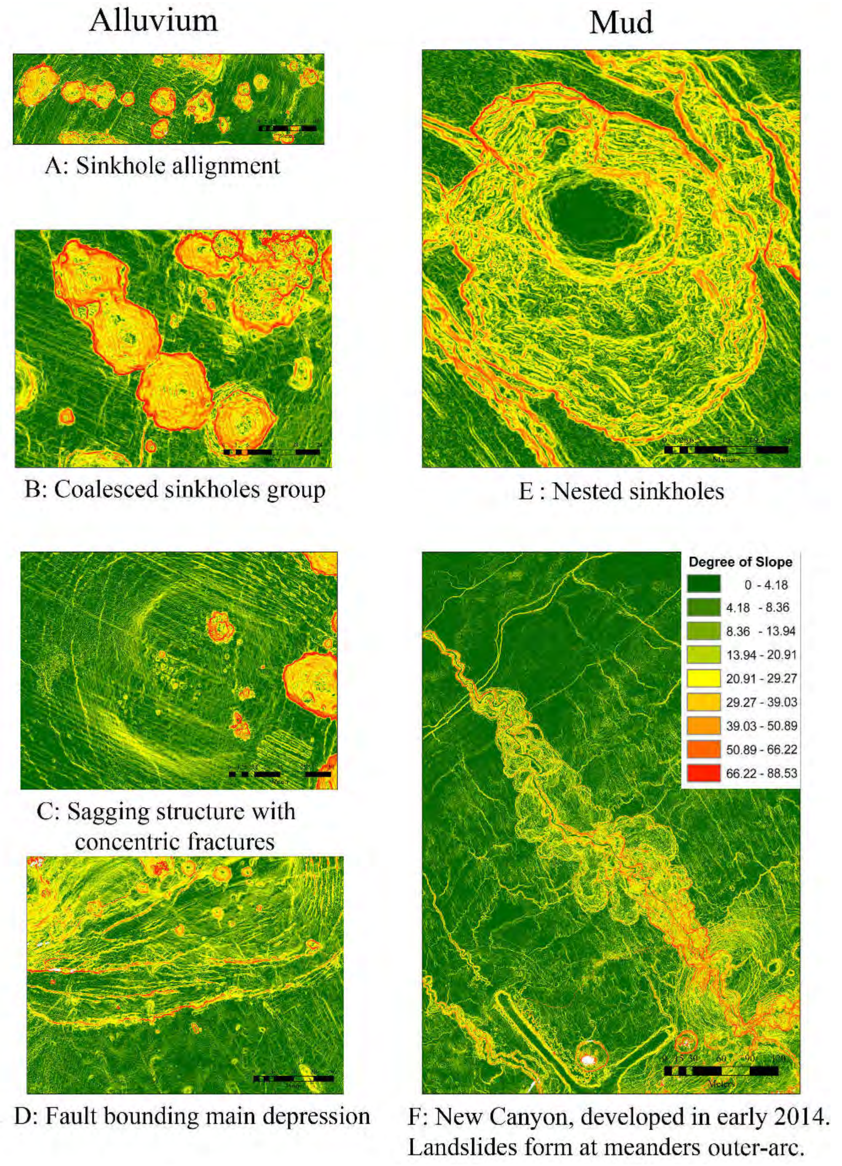

Figure 14: Slope maps of sinkholes (**A, B, E**), stream channels and related landslides (**F**), depression structures (**C**) as well as faults (**D**) derived from the DEM.

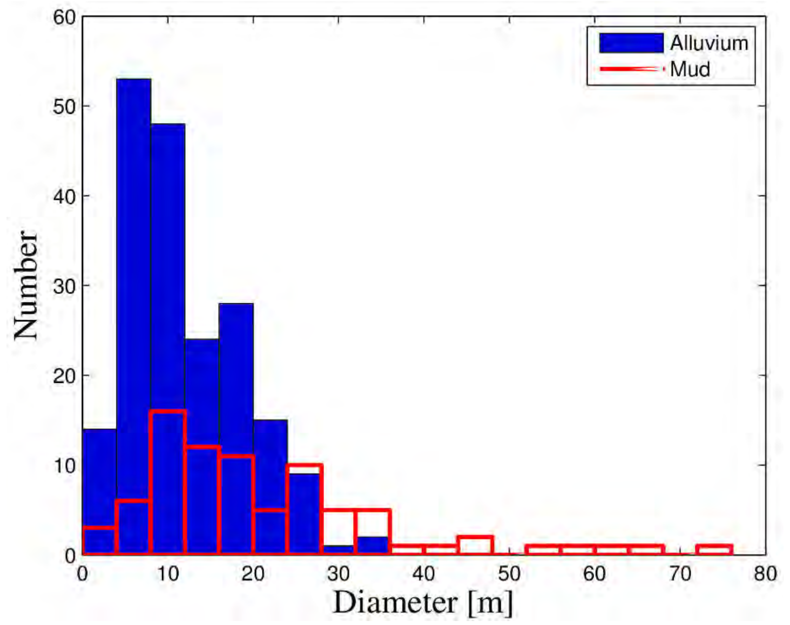

Figure 15: Histogram of sinkhole diameter distribution in alluvium (blue) and mud (red contours).

Subsidence at Ghor Haditha attains several distinct morphological expressions (**Fig. 14**). These appear to be largely material dependent (alluvium vs mud).

In alluvium, sinkholes generally show steeper internal slopes and in several places linear alignments or coalescence (**Fig. 14A, B**). More rarely, subsidence in the alluvium expresses locally as 'sag' structures with a wide 'halo' of concentric cracks (**Fig. 14C**). Numerous cracks and fault scarps are also observed at the boundary of the main depression (**Fig. 14D**).

In the mud, sinkhole alignments are not so obvious. Coalescence or 'nesting' of sinkholes is more cluster-like and many sinkholes display a wide, fractured zone of back-rotated strata (**Fig. 14E**). This is structurally and morphologically similar to landslides or slumps found adjacent to the deeper stream channels (**Fig. 14F**).

In total, we mapped 287 sinkholes in the surveyed area. About 65 % of these occur in the alluvium (**Fig. 15**). The mode of the sinkhole size distribution - diameter of about 10 m - is approximately the same in the alluvium and mud. However the sinkholes in the mud attain higher diameters overall as shown by their more skewed distribution (**Fig. 15**).

A clear result of this survey is that sinkholes in the alluvium deposits display a higher depth to diameter ratio ($\bar{D} = 0.4$) than those in the mud layers ($\bar{D} = 0.14$, see Figs. 16 and 17). This supports the idea that sinkhole morphology in the Ghor Haditha area is strongly controlled by the differing mechanical properties of the sediments in which they form.

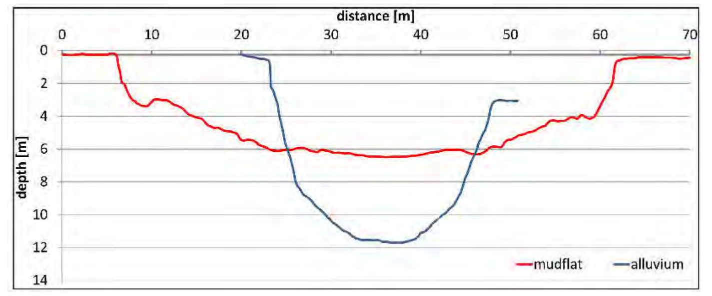

Figure 16: Topographic profiles across two representative sinkholes.

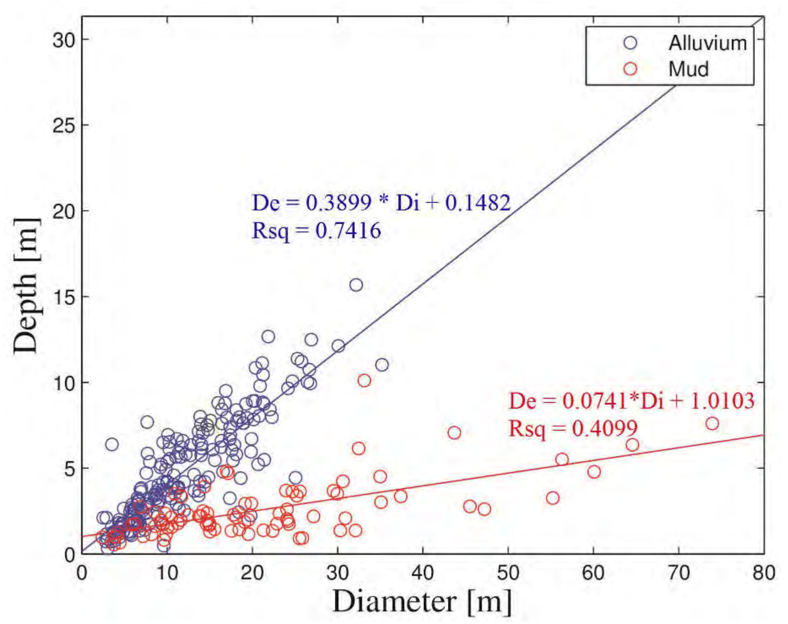

Figure 17: Statistical distribution of sinkhole D=De/Di ratios. Sinkholes in alluvium material show higher D ratios between 0.05 and 1.8 with a mean of 0.4 . Sinkholes based in the mud have values of D between 0.036 and 0.41 with a mean of 0.14 .

6. Summary

1 . The combination of field observations with a high-resolution, Near-field photogrammeteric survey provides new insights into land subsidence and sinkhole formation at Ghor Haditha, Jordan.

2 . Channelized ground water flow occurs at the contact between the mud and alluvium sequences and is regarded as one driving process for subsurface material depletion

3 . The sinkhole depth/diameter ratio (D) is generally greater in the mechanically stronger alluvial fan sediments than in the weaker muds of the former Dead Sea lakebed.

4 . Sinkhole morphology at Ghor Haditha is strongly controlled by the mechanical properties of the host sediments.

References

Harwin, S. and A. Lucieer. "Assessing the accuracy of georeferenced point clouds produced via multi-view stereopsis from Unmanned Aerial Vehicle (UAV) imagery". In: Remote Sensing 4 (2012), pp. 1573–1599.

Taqieddin, S. a., N. S. Abderahman, and M. Atallah. "Sinkhole hazards along the eastern Dead Sea shoreline area, Jordan: a geological and geotechnical consideration". In: Environmental Geology 39.11 (Oct. 2000), pp. 1237–1253.

Yechieli, Y., M. Abelson, A. Bein, O. Crouvi, and V. Shtivelman. "Sinkhole 'swarms' along the Dead Sea coast: Reflection of disturbance of lake and adjacent groundwater systems". In: Geological Society of America Bulletin 118.9-10 (Sept. 2006), pp. 1075–1087.